International Journal of Sustainable Built Environment (2016) 5, 370–386

HOSTED BY

ELSEVIER

Gulf Organisation for Research and Development

International Journal of Sustainable Built Environment

ScienceDirect
www.sciencedirect.com

CrossMark

Original Article/Research

A simulation study on performance evaluation of single-stage LiBr–H_2O vapor absorption heat pump for chip cooling

Manu S. [a,*], T.K. Chandrashekar [b]

[a] Department of Mechanical Engineering, Sri Siddhartha Institute of Technology, Tumkur 572105, Karnataka, India
[b] Department of Mechanical Engineering, Mangalore Institute of Technology and Engineering, Moodabidri-574225, Mangalore, Karnataka, India

Received 6 March 2016; accepted 21 August 2016

Abstract

The growth of Lithium Bromide–Water (LiBr–H_2O) absorption based heat pump is encouraged for the necessity of extracting high heat from the electronic chips. This paper presents a simulation study of single-stage LiBr–H_2O vapor absorption heat pump for chip cooling. In this study, a detailed thermodynamic analysis of the single-stage LiBr–H_2O vapor absorption heat pump for chip cooling in the nonexistence of solution heat exchanger was performed and a user-friendly graphical user interface (GUI) package including visual components was developed by using MATlab (2008b). The influence of chip temperature on COP (Coefficient of Performance), flow rates and conductance was examined by using the developed package. The model is validated by using the values available in the literature and indicates that there is a greater reduction in the absorber load. The influence of chip temperature on the performance and thermal loads of individual components was studied and it was concluded that, COP increases from 0.7145 to 0.8421 with an increase in chip temperature.

Keywords: LiBr–H_2O; Absorption heat pump; Chip cooling; Simulation

1. Introduction

Due to the advancement in semiconductor technology there is a rapid increase in the level of power density of the IC chips. These IC chips are working under harsh conditions having a high heat flux of 100 W/cm^2 at a junction temperature of more than 100 °C. Traditional convective air cooling methods are facing complications in extracting high heat flux and in maintaining the IC chips at ambient temperature below the restricted space assigned for thermal management. A number of attempts have been made to develop new alternate thermal solutions for chip cooling. Thermal solutions for chip cooling can be characterized as passive and active cooling methods. In passive cooling, working fluid is circulated by means of gravitational force or capillary method but in active cooling system circulation of the working fluid is by means of a pump or a compressor and improves the performance of the system.

Number of researchers developed passive and active cooling methods for device cooling. Tuckerman and Pease (1981) demonstrated the innovative method of cool-

* Corresponding author.
E-mail addresses: manussit1982@gmail.com (S. Manu), chandra_ssit@yahoo.co.in (T.K. Chandrashekar).
Peer review under responsibility of The Gulf Organisation for Research and Development.

http://dx.doi.org/10.1016/j.ijsbe.2016.08.002

Nomenclature

CR	circulation ratio
E	energy (kJ/s)
h	Enthalpy (kJ/kg)
K	thermal conductivity (W/mK)
LiBr–H_2O	Lithium Bromide–Water
LMTD	logarithmic mean temperature difference (°C)
$\dot{m}$	mass flow rate (kg/s)
P	pressure (bar)
$\dot{Q}$	rate of Heat transfer (kW)
R	thermal Resistance (°C/W)
S	shape factor
T	temperature (°C)
UA	conductance (kW/°C)
V	specific volume (m^3/kg)
$\dot{W}p$	pump power (kW)
X	concentration (%)

Subscript

a	Absorber
c	Condenser
e	Evaporator
g	generator
i	inlet
o	outlet
w	wall
ws	wall superheat
Δ	Difference

ing chips by having a single-row micro-channel etched directly into the back of a silicon wafer. Water is used as the working fluid and the maximum obtained power density of 790 W/m^2K is removed with a rise in water temperature of 71 K at a pressure of drop 2 bar. Pal et al. (2002) showed thermosyphon techniques for chip cooling using water as a working fluid and the maximum obtained cooling capacity of 80 W at average junction-to-ambient thermal resistance of 0.95 KW^{-1}.

Bin et al. (2012) developed copper based microchannel heat exchangers which are used in heat absorption segments, heat rejection segments and recirculating-liquid cooling system. The experimentation was performed on liquid-passing heat rejection segment and microchannel-based recirculating-liquid cooling system. The microchannel liquid flow through individual fins enhances the heat transfer performance. Copper base microchannel heat exchangers showed there is advantage in removing high heat flux under limited space. Bintoro et al. (2005) investigated jet impinging technique using water as working fluid to obtain a maximum cooling capacity of 200 W with a maximum junction temperature of 90 °C. Maydanik et al. (2005) studied the loop heat pipe where water and ammonia are the two working fluids, indicating a maximum cooling capacity of 130 W at minimum junction-to-ambient thermal resistance of 0.58 kW^{-1} is achieved. Jiang et al. (2002) showed electro-osmotic pumping using water as working fluid with a maximum cooling capacity of 38 W with a junction temperature below 120 °C and junction-to-ambient thermal resistance of 2.5 KW^{-1}. Fan et al., 2001) developed a thermoelectric micro-cooler with maximum cooling power density of 1 $kWcm^{-2}$. Tan and Tso (2004) conducted the experimental investigation for cooling of mobile electronic equipment using phase change materials. n-eicosane is used as a phase change material and is used to absorb heat from the chips and preserve the chip temperature at 50 °C but Hewitt et al. (2010) reviews the Phase Change Materials (PCMs) for latent heat thermal energy storage systems and showed the problems in formulating the system.

Mongia et al. (2006) developed vapor compression system at laboratory level using Isobutane as a refrigerant with a maximum cooling capacity of 50 W at junction-to-ambient thermal resistance of 0.25 K W^{-1} and COP of 2.25. Trutassanawin et al. (2006) carried out the experimental investigation on miniature-scale vapor compression refrigeration systems for cooling electronic devices, having capacities of 121–268 W for the pressure ratios of 1.9–3.2 and COP of 2.8–4.7. Chiriac and Chiriac (2010) constructed an analytical model using water-ammonia solution as working pair for microelectronic cooling and obtained maximum COP of 0.73. Kim et al. (2008) and Yoon et al. (2007) performed a theoretical study of an absorption based heat pump system for device cooling using LiBr–H_2O as working pair having a maximum cooling capacity of 100 W and COP of 0.87.

Ebrahimi et al. (2015) explained technical and economic problems of absorption cooling machines which are used in data centers. The study includes the development of the steady state model in order to do energy balance and exergy analysis. The innovative configuration was developed by placing a generator in place of a condenser on the chip cooling circuit. The simulation was performed for both absorption cooling systems such as LiBr–H_2O and water–ammonia. The LiBr–H_2O absorption scheme showed best system for data center/server operating conditions. The author concludes that, there is a need of sensitivity analysis for these types of systems.

LiBr–H_2O absorption pair showed its potential in extracting high latent heat and proved ecofriendly since water is used as refrigerant and LiBr–H_2O solution as absorption pair. From the last century, numerous experimental investigations were performed on LiBr–H_2O heat pump systems by many researchers. These experimental investigations are mainly devoted to enhance the performance of the system or to identify the critical parameters

that affect the performance. Mostafavi and Agnew (1996) studied the effect of ambient temperature on the generator temperature, concentration of strong solution, flow ratio of the solution and on the evaporator temperature for LiBr–H_2O absorption unit. Yoon et al. (2003) carried out an experimental examination on double-effect LiBr–H_2O absorption cycle.

Asdrubali and Grignaffini (2005) and Aphornratana and Sriveerakul (2007) experimentally examined the performance of an absorption chiller with a cooling capacity of 2 kW. The outcomes indicated that the performance of the scheme rises with the rise of the generator and evaporator inlet temperature. The performance of the chiller decreases with the rise in the condenser and absorber inlet temperature. Marc et al. (2010) and Pongtornkulpanich et al. (2008) experimentally studied the performance of a solar-absorption A/C system with a cooling capacity of 10 kW operating in Italy. Melograno et al. (2009) developed an experimental test opportunity capable of gathering performance curves from an absorption chiller with cooling capacity up to 20 kW. Agyenim et al. (2010) experimentally tested the performance of solar-absorption A/C systems of capacity 4.5 kW. The test showed the average COP of 0.48 for an average peak solar insolation of 812 W/m^2. The performance data for specific operating conditions were mapped.

Extensive literature is available related to the development of simulation models to guess the performance of LiBr–H_2O in diverse operating conditions and for different applications. Joudi and Lafta (2001) developed a steady state computer simulation model in order to predict the influence of several operating situations on the function of each component and to find the performance of an absorption refrigeration system using LiBr–H_2O as a working pair.

Grossman and Zaltash (2001) developed a computer code ABSIM (Absorption Simulation) for the simulation of absorption schemes in a flexible and modular form making it likely to examine numerous cycle configurations with different working fluids.

Alva and Gonzalez (2002) and Atmaca and Yigit, 2003 established the mathematical model for the absorption chiller with a capacity of 10.5 kW to determine the performance characteristics of the system. Florides et al. (2003) developed the mathematical model based on energy balance equations written for the absorber, condenser, evaporator and generator for an absorption cooling capacity of 1 kW. Mehrabian and Shahbeik (2005) developed the computer program for the design and thermodynamic analysis of a single effect absorption chiller using LiBr–H_2O solution as working fluid.

In recent decades, there was greater attention in applying the principles of second law of thermodynamics for evaluating and assessing the thermodynamic performance of LiBr–H_2O system. Talbi and Agnew (2000) performed exergy analysis on a single-effect absorption refrigeration cycle using LiBr–H_2O as the working fluid pair. Lee and Sherif (2000) performed a second law analysis of a single effect LiBr–H_2O absorption refrigeration system. The influence of heat source temperature on COP and exergetic efficiency was evaluated. Martinez et al. Martinez and Pinazo, 2002 utilized the statistical tool to find the influence of variation of heat exchanger areas on the performance of a single effect machine.

Sencana et al. (2005) analyzed the exergy losses in each component of a single stage LiBr–H_2O absorption system. He compares exergy losses of generator and absorber with the evaporator and condenser. The exergetic efficiency of the system drops with an increase in heat source temperature for both cooling and heating applications. Sedighi et al. (2007) made the exergy analysis of a single-effect LiBr–H_2O absorption refrigeration system. The exergy analysis was performed by taking the mass and energy conservation into consideration with respect to the first and second laws of thermodynamics. The results showed that, a decrease in cooling water temperature causes an enhancement in the COP and Exergetic Coefficient of Performance (ECOP). Rising the evaporator temperature also improves the COP; however it caused a decrease in the ECOP of the system.

The literature reviews of the authors like Vargas et al. (1988), Yang and Guo (1987), Atilgan and Aygun (2014), Agrawal et al., (2015), Karno and Ajib (2008) and Iranmanesh and Mehrabian (2012) have showed in their studies on LiBr–H_2O absorption heat pump with respect to development, modification of the cycle, alternate working pair and simulation used for different applications coupled to different energy sources.

In a review of an extensive literature no attempt has yet been made to study the performance of LiBr–H_2O based absorption heat pump for chip cooling. The present work aims to study the performance of LiBr–H_2O based absorption heat pump especially for chip cooling. The steady state simulation (analytical) model was developed to analyze the influence of chip temperature on coefficient of performance, load, mass flow rate and conductance. A user-friendly graphical user interface (GUI) package including visual components for simulating the performances of absorption refrigeration systems working for chip cooling is developed by using MATlab (2008b) software. It is expected that the user-friendly software package developed would help the researchers in calculation of performance and determination of suitable operating conditions. The software package helps in determining the effect of chip temperature on performance, loads, flow rates and conductance at a fast rate with high accuracy.

2. Mathematical model of absorption heat pump for chip cooling

In this study, the evaporator of single-effect LiBr–H_2O absorption based heat pump is placed directly on the back of a chip as shown in Figs. 1 and 2 thereby maintaining the

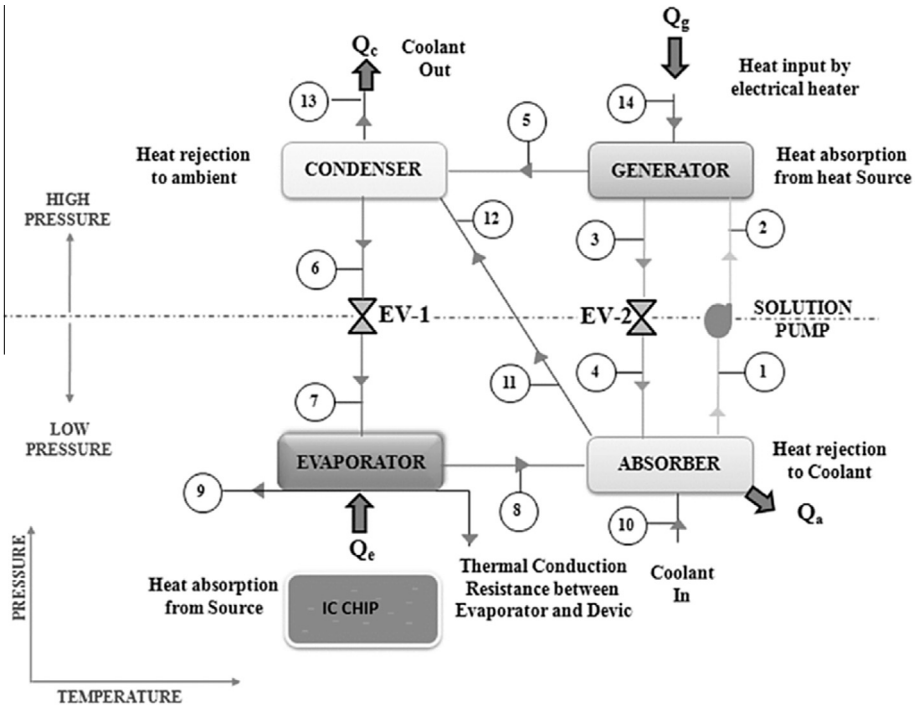

Figure 1. Absorption based heat pump system for chip cooling.

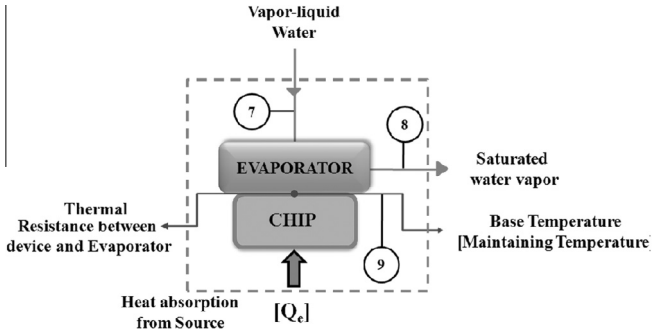

Figure 2. Schematic of chip coupled evaporator.

chip temperature at ambient level. In the LiBr–H_2O absorption based heat pump system, water is used as refrigerant and LiBr–H_2O as an absorption pair. The saturated liquid refrigerant coming from the expansion valve (State 7) is vaporized by absorbing the heat dissipated from the chip (State 8). The refrigerant vapor coming from evaporator is exothermically condensed and absorbed into the strong LiBr–H_2O solution (state point 4) i.e. weak in water percentage, resulting in weak LiBr–H_2O solution i.e. rich in water percentage at state point 1.The rejected heat is absorbed by the coolant water as shown in Fig. 1. LiBr–H_2O solution is pressurized by the solution pump (State 2). In the generator, the high pressure and high temperature superheated refrigerant water vapor is created and desorbed from the weak LiBr solution and returns to the refrigerant loop. The superheated water vapor condensed in the condenser and the rejected latent heat is absorbed by the coolant water as shown in Fig. 1.

Assumptions

- Pipe pressure drops are negligible.
- The heat gain to the evaporator from the surroundings and the heat losses from the generator to the surroundings are negligible.
- In the expansion process, the enthalpy is constant.
- The water leaving the generator will be superheated vapor, water leaving the condenser will be saturated liquid and water leaving the evaporator is saturated vapor.
- The pressure in the generator is the same as the condenser (saturation pressure) and pressure in the evaporator is the same as the absorber (saturation pressure).
- The temperature difference in the condenser, evaporator, absorbent, and generator is negligible.
- The coolant outlet temperature from the absorber is the average temperature of inlet and outlet temperature of the coolant from the system.
- Temperature of the vapor refrigerant leaving the generator is the average temperature of inlet and outlet temperature of the solution entering and leaving the generator.
- Thermo physical properties of refrigerant with temperature and pressure remain constant.

2.1. Evaporator analysis

Fig. 2 illustrates the evaporator of single-effect LiBr–H_2O absorption based heat pump which is etched directly into the back of a chip. The refrigerant reaches the evapo-

rator in saturated liquid form and leaves as saturated vapor as shown in the Fig. 2 by absorbing the heat which is dissipated from the chip. The size of the evaporator used in chip cooling applications is relatively small and extensive literatures are available on the design of an evaporator. Number of researchers like Ribeiro et al. (2010), Qi et al. (2009), Mudawar and Weilin (2005), Mudawar (2011), Coggins et al., (2006), França et al. (2014), Francis et al., (2002) and Cunha et al. (2007) showed the potential of small parallel channels or microchannels for desired cooling capacity for chip cooling. Complete thermal conductance model has been formulated for the evaporator with the axis symmetry. The total thermal resistance of the evaporator is $R_{Contact}$ and $R_{Conduction}$ without considering convective resistance as shown in Fig. 3. The goal of the simulation is to find the influence of chip temperature on COP, load, mass flow rate and conductance of the heat exchangers. The input data are: Chip temperature (T_9), Total resistance (R), Inlet cooling water temperature (T_{10}), Approaching temperature of evaporator or difference in temperature from chip to evaporator (ΔT_1), Approaching temperature of absorber (ΔT_2), Approaching temperature of condenser (ΔT_3), Approaching temperature of generator (ΔT_4), evaporator wall superheat (ΔT_{WSe}), generator wall superheat (ΔT_{WSg})and Concentration difference (ΔX). A typical loop of calculations can begin from point 8, whose temperature is estimated from the input information. Assuming steam leaving the evaporator will be dry saturated, the pressure in evaporator is same as the absorber. The typical calculation is given as follows:

$$T_8 = T_9 - \Delta T_1 \tag{1}$$

$$\Delta T_1 = (T_9 - T_{We}) + (T_{We} - T_8) \tag{2}$$

$$\Delta T_1 = (T_9 - T_{We}) + \Delta T_{WSe} \tag{3}$$

where, (ΔT_{WSe}) is the evaporator wall superheat and as shown in Fig. 3. The evaporator wall superheat is assumed to be less than the approaching temperature of evaporator.

Wall or surface temperature of the evaporator is given by

$$T_{We} = T_8 + \Delta T_{WSe} \tag{4}$$

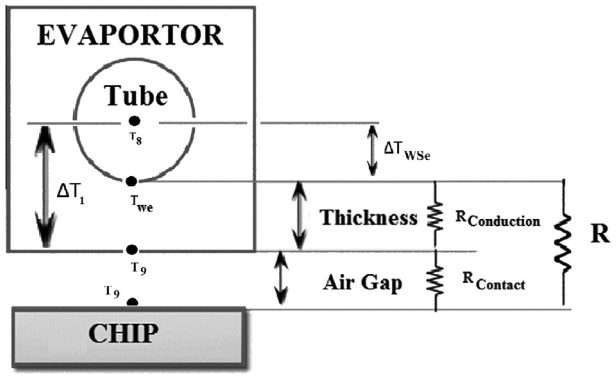

Figure 3. Shows thermal analysis of evaporator.

In many circumstances, two-dimensional or three-dimensional conduction troubles are solved using present solutions to the heat diffusion equation. The solutions are stated in terms of a shape factor, S, by Incopera et al. (2007) That is, the heat transfer rate can be expressed as

$$\dot{Q}_e = SK(T_9 - T_{We}) \tag{5}$$

where, ($T_9 - T_{We}$) is the temperature change among the chip and the wall as shown in Fig. 2. The two-dimensional conduction resistance can be stated as:

$$R_{Conduction} = 1/SK \tag{6}$$

Then $\dot{Q}_e$ becomes,

$$\dot{Q}_e = (T_9 - T_{We})/R_{Conduction} \tag{7}$$

But, it is essential to identify that, in chip cooling, the temperature fall through the interface among sinks might be considerable. This temperature alteration is due to the thermal contact between the evaporator and the chip and is known as the thermal contact resistance $R_{contact}$. Then total thermal resistance (R) becomes,

$$R = R_{Conduction} + R_{contact} \tag{8}$$

Evaporator load is given by:

$$\dot{Q}_e = \frac{T_9 - T_{We}}{R} \tag{9}$$

$$T_7 = T_8 \tag{10}$$

$$P_7 = P_1 = P_4 = P_8 = f(T_8) \tag{11}$$

$$h_8 = f(T_8) \tag{12}$$

$$h_7 = h_6 = f(T_7) \tag{13}$$

The mass flow rate of refrigerant from the evaporator is evaluated from the input data

$$\dot{m}_7 = \dot{m}_6 = \dot{m}_5 = \dot{m}_8 = \frac{\dot{Q}_e}{(h_8 - h_7)} \tag{14}$$

To determine the conditions at point 7, the absorber and generator must be analyzed, but T_{11} is not known and it was guessed. The temperature at point 1 can be calculated by:

$$T_1 = T_{11} + \Delta T_2 = T_2 \tag{15}$$

Concentration of the solution leaving the absorber is given by:

$$X_1 = X_2 = f(P_8, T_1) \tag{16}$$

The enthalpy of the solution leaving the absorber and pump remains same and is given by:

$$h_1 = h_2 = f(T_1, X_1) \tag{17}$$

From the assumption, Coolant water leaving the condenser is given by:

$$T_{13} = (T_{11} \times 2) - T_{10} \tag{18}$$

The condensing temperature of the refrigerant is given by:

$$T_6 = T_{13} + \Delta T_3 \quad (19)$$

The condensing pressure of the refrigerant is given by:

$$P_6 = P_5 = P_2 = P_3 = f(T_6) \quad (20)$$

The enthalpy of the superheated vapor refrigerant leaving the generator is given by:

$$h_5 = f(T_6, P_6) \quad (21)$$

Concentration of the solution leaving the generator is given by:

$$X_3 = (X_1 + \Delta X) \quad (22)$$

Solution temperature leaving the generator is given by:

$$T_3 = f(X_3, P_6) \quad (23)$$

Enthalpy of the solution leaving the generator is given by:

$$h_3 = h_4 = f(T_3, X_3) \quad (24)$$

The heater temperature of the generator is given by:

$$T_{14} = T_3 + \Delta T_4 \quad (25)$$

Approaching temperature in the generator is given by:

$$\Delta T_4 = (T_{14} - T_{WSg}) + (T_{WSg} - T_3) \quad (26)$$

$$\Delta T_4 = (T_{14} - T_{wsg}) + \Delta T_{WSg} \quad (27)$$

where, ΔT_{WSg} is the generator wall superheat as shown in Fig. 4.

From assumption, temperature of the vapor refrigerant leaving the generator is given by:

$$T_5 = (T_1 + T_3) \times 0.5 \quad (28)$$

Circulation Ratio (CR) is given by:

$$CR = \frac{X_1}{(X_3 - X_1)} \quad (29)$$

Mass flow rate of weak solution leaving the absorber is given by:

$$\dot{m}_1 = \dot{m}_2 = \left(\frac{X_3}{(X_3 - X_1)}\right) \times \dot{m}_8 \quad (30)$$

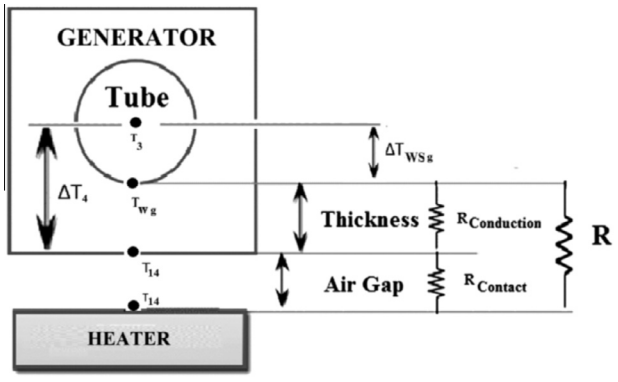

Figure 4. Shows thermal analysis of generator.

Mass flow rate of strong solution leaving the generator is given by:

$$\dot{m}_3 = \dot{m}_1 - \dot{m}_5 \quad (31)$$

Temperature of the strong solution entering the generator is given by:

$$T_4 = f(X_3, P_8) \quad (32)$$

The heat balance on the absorber is given by:

$$\dot{Q}_a = (\dot{m}_8 \times h_8) + (\dot{m}_4 \times h_4) - (\dot{m}_1 \times h_1) \quad (33)$$

The heat balance on the condenser is given by:

$$\dot{Q}_c = \dot{m}_5 \times (h_5 - h_6) \quad (34)$$

Total heat rejected from the system is given by:

$$E_o = \dot{Q}_a + \dot{Q}_c \quad (35)$$

Coolant mass flow rate is given by:

$$\dot{m}_{13} = \dot{m}_{10} = \dot{m}_{11} = \dot{m}_{12} = \frac{E_o}{(Cp \times (T_{13} - T_{10}))} \quad (36)$$

The temperature of cooling water at absorber outlet is then,

$$T_{11} = T_{12} = \left(\frac{\dot{Q}_a}{(Cp \times M_{10})} + T_{10}\right) \quad (37)$$

This temperature is currently related to the value predicted in equation (15). The simulation is repeated till the last value is near enough to the preliminary value as shown in Fig. 5.The heat balance in the generator is given by,

$$\dot{Q}_g = (\dot{m}_3 \times h_3) + (\dot{m}_5 \times h_5) - (m_2 \times h_2) \quad (38)$$

Wall or surface temperature of the generator is given by:

$$T_{Wsg} = T_{14} - (\dot{Q}_g \times R) \quad (39)$$

Once the calculation of thermodynamic properties at all the state points of the cycle is carried out, easily design specifications can be obtained. The thermal load, logarithmic mean temperature variation and conductance for the evaporator, condenser, absorber, and generator are determined according to the subsequent formulation. Every unit is considered as a counter flow heat exchanger; because of this logarithmic mean temperature variation is used.

Typical Logarithmic mean temperature difference of evaporator is as shown in Fig. 6 and is given by:

$$LMTD_e = \frac{((T_9 - T_8) - (T_{We} - T_8))}{\log((T_9 - T_8)/(T_{We} - T_8))} \quad (40)$$

Conductance for the evaporator is given by:

$$UA_e = \frac{\dot{Q}_e}{LMTD_e} \quad (41)$$

Typical Logarithmic mean temperature difference of generator is as shown in Fig. 6 and is given by:

$$LMTD_g = \frac{((T_{14} - T_3) - (T_{Wsg} - T_3))}{\log((T_{14} - T_3)/(T_{Wsg} - T_3))} \quad (42)$$

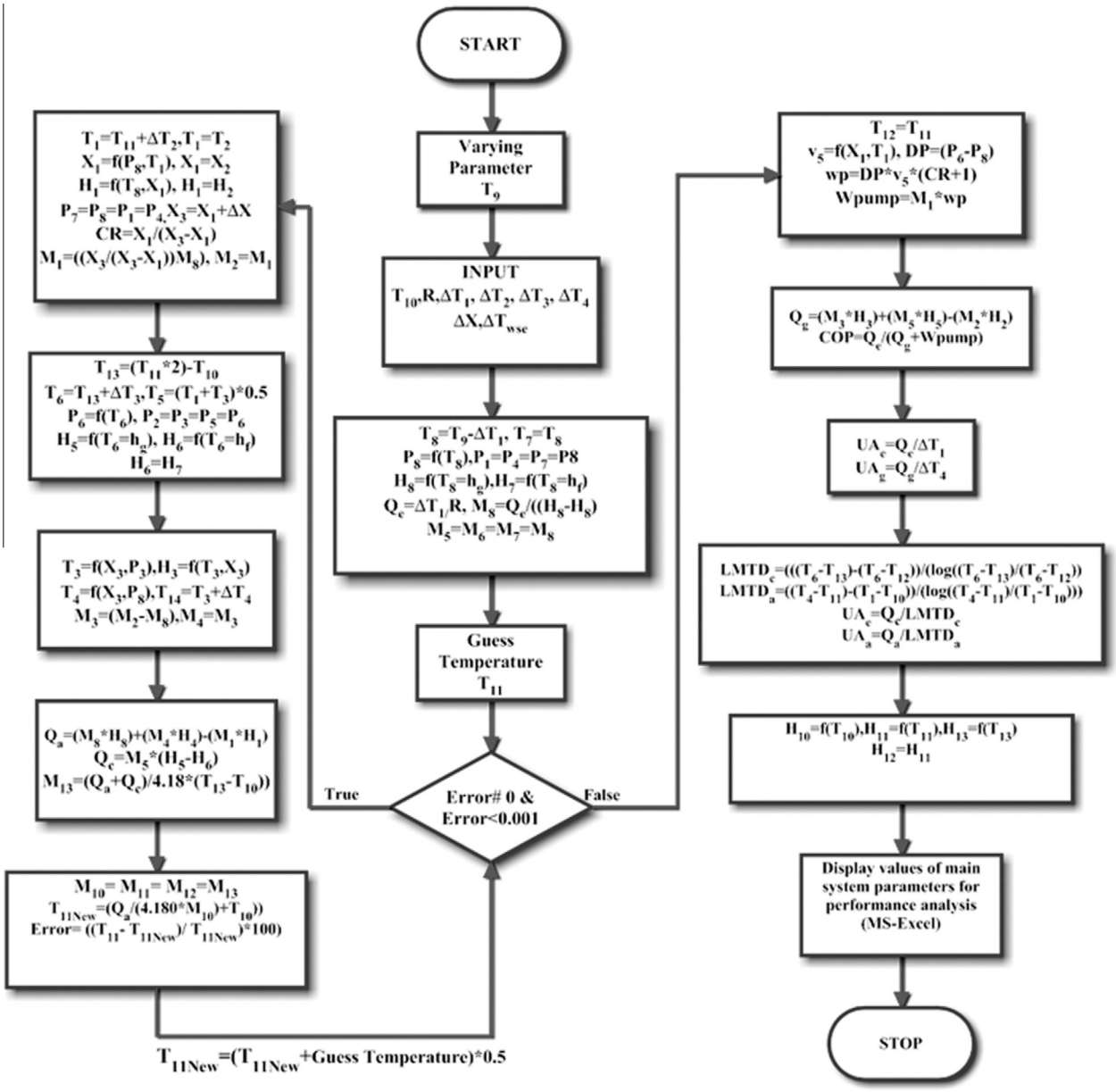

Figure 5. Flow chart of the simulation for varying base temperature.

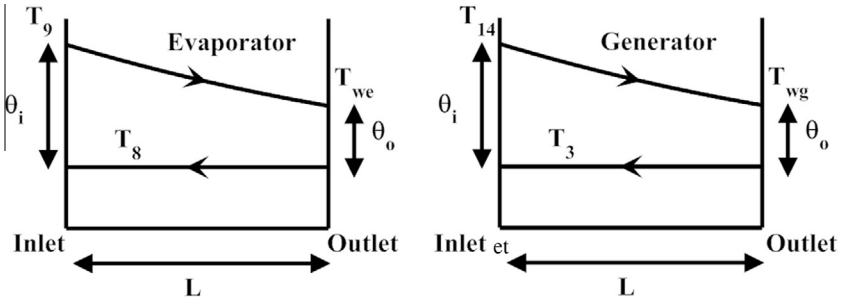

Figure 6. Temperature profile for evaporator and generator.

Conductance for the generator is given by:

$$UA_g = \frac{\dot{Q}_g}{LMTD_g} \tag{43}$$

Logarithmic mean temperature difference of condenser is given by:

$$LMTD_C = \frac{((T_6 - T_{13}) - (T_6 - T_{12}))}{\log((T_6 - T_{13})/(T_6 - T_{12}))} \tag{44}$$

Conductance for the absorber is given by:

$$UA_c = \frac{\dot{Q}_c}{LMTD_C} \tag{45}$$

Logarithmic mean temperature difference of absorber is given by:

$$LMTD_a = \frac{(T_4 - T_{11}) - (T_1 - T_{10})}{\log(T_4 - T_{11})/(T_1 - T_{10})} \tag{46}$$

Conductance for the absorber is given by:

$$UA_a = \frac{\dot{Q}_a}{LMTD_a} \tag{47}$$

Pump work is given by:

$$\dot{W}p = (P_6 - P_8) \times V_5 \times (CR + 1) \tag{48}$$

COP is given by:

$$COP = \frac{\dot{Q}_e}{(\dot{Q}_g + \dot{W}_p)} \tag{49}$$

The simulation starts from one state point in the cycle by determining pressure, temperature and enthalpy and continues to the subsequent state point. In order to analyze the complete cycle, it is essential to carry out a fixed point iteration for T_{11}. The ultimate values for these properties are assessed based on physical reasoning and compared with the preliminary predicted values. If the final value is not same as the initial value, the simulations are repeated as shown in Fig. 5.

3. Software program

The simulation executes the single-effect LiBr–H_2O based absorption based heat pump for chip cooling estimated based on the polynomial expressions developed to connect experimental vapor–liquid equilibrium and particular enthalpy– concentration information for LiBr–H_2O solutions. This is the renowned dominance of this program as associated with other simulations which experience lack of exact thermo-physical information. The thermo-physical properties of water were developed in MAT lab (2008b) by Holmgren (2006). Cantarutti et al. (2011) developed MAT lab code for the properties of LiBr–H_2O solution. These functions were used to develop the Graphical User Interface (GUI). The developed GUI contains screens as follows: the Input Page where the chip temperature, approaching temperatures, concentration difference, Total resistance is entered and variation of COP with chip temperature can be observed in the same page and the Output Page-1 shows the variation of thermal load, pressure, temperature, mass flow rates, LMTD and conductance with chip temperature can be seen. As an instance, the Input Page is shown in Fig. 7 and Output page is show in Fig. 8. The flow chart of the software program is shown in Fig. 5. The corresponding input and output data are shown in Tables 7–10.

4. Validation of the model

The current model was validated by comparing the results which are available in the literature. The comparative study of COP_E (Enthalpy based Coefficient of Performance) variation of the generator temperature is as shown in Fig. 9. In this simulation, the subsequent data have been used: $T_e = 2\ °C$, $T_c = T_a = 30\ °C$ and effectiveness of the solution heat exchanger was kept zero. It can be perceived that, as expected, the COP_E value raises with a rise in generator temperature, and the results achieved from the current simulation model are in better agreement with the results of Romera et al. (2000). The small variation can be attributed to the alteration among the data sets used for the thermodynamic properties.

The model is further verified and validated by using the reference information from the available literature in which the generator temperature is nearer to that of the waste heat temperature in liquid-cooled or two phase cooled data centers (Ebrahimi et al., 2015). Table 1 shows the values of input information from two references used for the model verification (Ebrahimi et al., 2015; Rubio-Maya et al., 2012). Tables 2 and 3 show the validation results. As seen from Table 2, the deviation among present model results and those of Rubio-Maya et al. (2012) result is lower than 10%. The deviations are due the model's differences in computing refrigerant properties as well as density and specific heat of the solution. The comparison shows good agreement among the present model and that of Rubio-Maya et al. (2012) model. In the second verification indicated in Table 3, the deviation among present model results and those of Ebrahimi et al. (2015) is lower than 10% for the entire load but, there is a greater reduction in the absorber load up to 10%. The comparison displays good agreement between the present model and that of Ebrahimi et al. (2015) model.

The verification of the model is continued, the model is executed using reference information from the open literature in which the absorption heat pump having series of coolant flow. Table 4 shows the values of input information from the references used for the model verification (Joudi and Lafta, 2001). Table 5 shows a comparison among the present model and reference models with respect to all the state points. It is observed from the Table 5, that the deviation among present model results and those of Joudi and Lafta (2001) is lower than 5% with respect to temperature, mass flow rate and concentration but there is greater

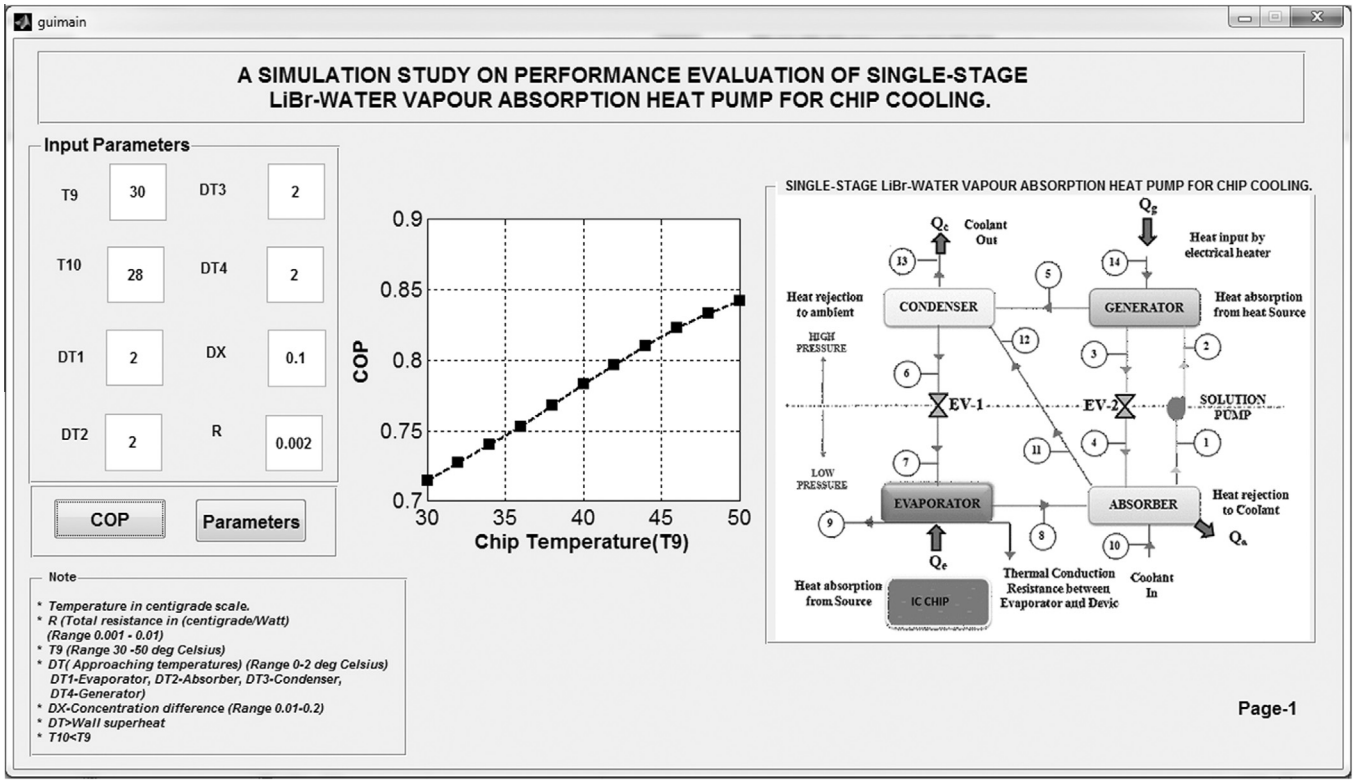

Figure 7. The Input Page of the GUI.

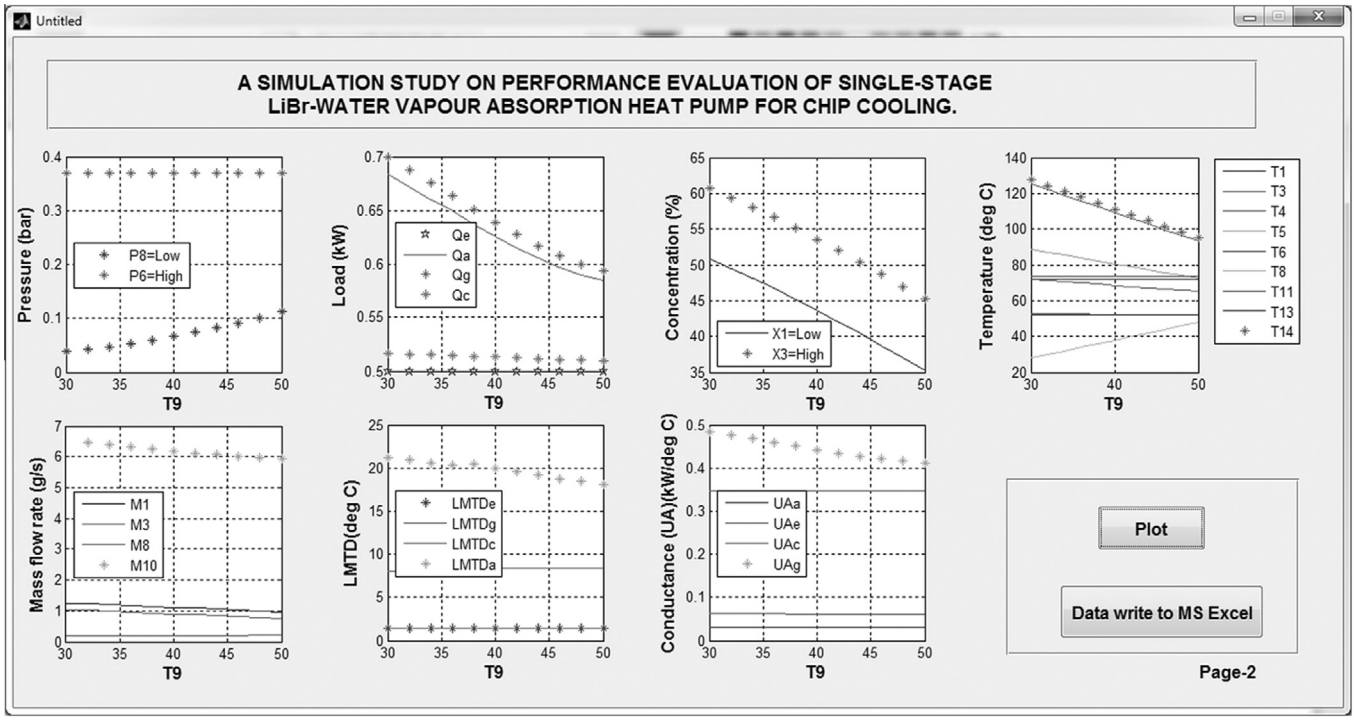

Figure 8. The Output Page of the GUI.

reduction of coolant flow rate up to 16%. As seen from Table 6, the deviation among present model results and those of Joudi and Lafta (2001) is lower than 3.51% for the entire load but there is a greater reduction of the absor-

Table 1
Input data from the reference models.

Variable	Ebrahimi et al. (2015)	Rubio-Maya et al. (2012)
Evaporator cooling load (kW)	201.29	201.29
Generator temperature (kW)	84.8	84.8
Condenser temperature (°C)	39.8	39.8
Evaporator temperature (°C)	8.6	8.6
Absorber temperature (°C)	35.5	35.5
Solution heat exchanger effectiveness (%)	70.7	70.7

ber load up to 10%. The comparison results show good agreement between the present model and that of Joudi and Lafta (2001) model.

5. Simulation results and discussion

This paper shows the results of the simulation program to examine the performance and design characteristics of single effect LiBr–H_2O based absorption refrigeration cycles. A typical (Chip temperature = 30 °C) absorption heat pump is examined based on the developed model. A set of input information is listed in Table 1. The corresponding output data are shown in Tables 2–4. The following results are obtained.

5.1. Effect of chip temperature on COP

Fig. 10 shows the system COP increasing from 0.7145 to 0.842 as T_9 (Chip temperature) is increased. This is due to a decrease in the CR from 5.0762 to 3.5273 as shown in Fig. 11 and increase in T_8 i.e. evaporator temperature from 20 to 40 °C. Kaynakli and Kilic (2007) showed that the COP increases as CR decreases. Eisa et al. (1986), Eisa and Holland (1986) and García Cascales et al. (2011) showed that the COP increases as evaporator temperature increases, and the best COP is obtained with T_1 (Absorber temperature) and T_6 (Condenser temperature). Also, Eisa et al. (1986) and Eisa and Holland (1986) verified experimentally that, with an increase in evaporator temperature there is an improvement of COP. The results of Fig. 10 the current model are in better agreement with results of references (Kaynakli and Kilic, 2007; Eisa et al., 1986; Eisa and Holland, 1986; García Cascales et al., 2011).

Table 4
Input data from the reference models.

Variable	Khalid Joudi et al.
Evaporator cooling load (kW)	211.1
Approaching temperature of evaporator (ΔT_1) (°C)	2.3
Approaching temperature of absorber (ΔT_2) (°C)	0.8000
Approaching temperature of condenser (ΔT_3) (°C)	2
Approaching temperature of generator (ΔT_4) (°C)	6
Concentration difference (°C)	0.0140
Mass flow rate of strong solution entering to the absorber (kg/s)	7.94
Concentration of weak solution entering to the absorber (%)	55.2
Temperature of weak solution entering to the absorber (°C)	36.1
Mass flow rate of weak solution entering to the generator	7.94
Circulation ratio	46.2426
Coolant water inlet temperature	30

5.2. Effect of chip temperature on thermal load

Fig. 12 demonstrates the variations of the thermal load as a function of T_9 at a constant approaching temperatures and constant inlet cooling water temperature of 28 °C. It can be observed from this figure that when T_9 increases, there is a decrease in generator load ($\dot{q}_g$) from 0.6996 to 0.5936 kW, absorber load ($\dot{q}_a$) from 0.6830 to 0.5842 kW, condenser load ($\dot{q}_c$) from 0.5166 to 0.5095 kW and pump work ($\dot{W}p$) from 0.015 to 0.0081 W which can be observed from Fig. 11 this is due to decrease in Kaynakli and Kilic (2007) showed that, ($\dot{q}_g$), ($\dot{q}_a$), ($\dot{q}_c$) and ($\dot{W}p$) loads decreases as CR decreases. Aphornratana and Sriveerakul (2007) ver-

Table 2
Verification of present model by comparing simulation results of Rubio-Maya et al. (2012).

Variable	Present study	Rubio-Maya et al. (2012)	Deviation (%)
Generator heat flow rate (kW)	258.4151	259.55	0.43
Condenser heat flow rate (kW)	205.8763	213.37	3.51
Absorber heat flow rate (kW)	253.017	247.47	2.24
Coefficient of Performance	0.7789	0.7755	0.43

Table 3
Verification of present model by comparing simulation results of Ebrahimi et al. (2015).

Variable	Present study	Ebrahimi et al. (2015)	Deviation (%)
Absorber heat flow rate (kW)	253.017	241.345	4.83
Generator heat flow rate (kW)	258.415	246.207	4.95
Condenser heat flow rate (kW)	205.8763	206.155	0.135
Coefficient of Performance	0.7789	0.8175	4.72

Table 5
Verification of model by comparing results with those of Joudi and Lafta (2001).

Sl. No	Parameters	Temperature (°C)			Mass flow rate (kg/s)			Concentration (%)		
		Joudi and Lafta (2001)	Present Study	Deviation (%)	Joudi and Lafta (2001)	Present Study	Deviation (%)	Joudi and Lafta (2001)	Present Study	Deviation (%)
1	Chilled water inlet to evaporator	12.00	12.00	0.00	10.08	10.08	0.00			
2	Chilled water outlet from evaporator	8.00	8.00	0.00	10.08	10.08	0.00			
3	Vapor evaporator to absorber	5.70	5.70	0.00	0.089	0.0849	4.60			
4	Weak solution outlet from absorber	33.10	33.1	0.00	8.03	7.756	3.41	54.60	54.23	0.67
5	Weak Solution outlet from solution pump	33.10	33.1	0.00	8.03	7.756	3.41	54.60	54.23	0.67
6	Weak Solution inlet to solution heat exchanger	33.10	33.1	0.00	4.015	4.015	0.00	54.60	54.23	0.67
7	Weak solution inlet to generator	66.53	66.53	0.00	4.015	4.015	0.00	54.60	54.23	0.67
8	Strong solution outlet from the generator	74.00	73.32	0.91	3.92	3.92	0.00	56.00	55.63	0.67
9	Inlet hot water to generator	85.00	85.00	0.00	14.10	14.10	0.00			
10	Outlet hot water from generator	80.00	80.00	0.00	14.10	14.10	0.00			
11	Strong solution outlet from Heat exchanger	39.17	39.17	0.00	3.93	3.93	0.00	56.00	55.63	0.67
12	Weak Solution outlet from solution sump	33.10	33.10	0.00	4.02	4.02	0.00	54.60	54.23	0.67
13	Intermediate Solution Inlet to absorber	36.10	36.10	0.00	7.94	7.94	0.00	55.20	55.20	0.00
14	Vapor from generator to condenser	38.00	69.92	84.0	0.089	0.0849	4.60			
15	Condensate from condenser to expansion device	38.00	38.78	2.05	0.089	0.0849	4.60			
16	Inlet cooling Water to absorber	30.00	30.00	0.00	20.10	17.05	15.17			
17	Outlet cooling water from absorber	33.39	33.67	0.83	20.10	17.05	15.17			
18	Outlet cooling water from condenser	36.00	36.78	2.10	20.10	17.05	15.17			

ified experimentally that,($\dot{q}_g$), ($\dot{q}_a$), ($\dot{q}_c$) and ($\dot{W}p$) loads decrease as CR decreases but evaporator load ($\dot{q}_e$) remains constant as 0.5000 kW this is due to constant in ΔT_1 as 2 °C. Chaudhari et al. (1985) validated experimentally that (q_e) nearly remains constant with a rise in evaporator temperature. The results of Figs. 11 and 12 are valid with the theoretical and experimental of references (Kaynakli and Kilic, 2007; Aphornratana and Sriveerakul, 2007; Chaudhari et al., 1985).

5.3. Effect of chip temperature on concentration

Fig. 13 demonstrates the variations of the concentration as a function of T_9 at a constant approaching temperatures and constant in inlet cooling water temperature of 28 °C. There is a significant effect of T_9 on the concentrations and the weak solution coming from the absorber ($X_w = X_1$) decreases from 50.76 to 35.27%, this is because of an increase in evaporator pressure (P_8). Kaynakli and Kilic (2007) and Chaudhari et al. (1985) experimentally showed that, an increase in solution pressure (evaporator pressure) decreases the concentration of the weak solution coming from the absorber. Similarly, there is a reduction in concentration of strong solution entering from the generator ($X_s = X_3$) from 60.76% to45.27%, this is due to a constant concentration difference ($\Delta X = X_3 - X_1 = 0.1$). The results of Fig. 13 are in good agreement with the theoretical and experimental of references (Kaynakli and Kilic, 2007; Chaudhari et al., 1985).

5.4. Effect of chip temperature on system temperature and pressure

Fig. 14 demonstrates variations of the pressure as a function of T_9 at constant approaching temperatures and constant inlet cooling water temperature at 28 °C. As T_9 increases, there is an increase in P_8 from 0.0378 to 0.1117 bar this is due to an increase in T_8 from 20 to 48 °C. Joudi and Lafta (2001) showed that, as the evaporator temperature increases there is an increase in evaporator

Table 6
Verification of model by comparing simulation results of Joudi and Lafta (2001).

Variable	Present study	Joudi and Lafta (2001)	Deviation (%)
Evaporator heat flow rate (kW)	211.1	211.1	0
Absorber heat flow rate (kW)	261.92	285	8.09
Generator heat flow rate (kW)	293.26	296.3	1.02
Condenser heat flow rate (kW)	221.61	221.7	0.040
Coefficient of Performance	0.7168	0.71	0.95

Table 7
List of Input parameters for varying chip temperature.

Sl.No	Parameter	Symbol	Value	Unit
1	Base temperature	T_9	**30**	°C
2	Total resistance	R	0.002	°C/W
3	Inlet cooling water Temperature	T_{10}	28	°C
4	Approaching Temperature of Evaporator	ΔT_1	2	°C
5	Approaching Temperature of Absorber	ΔT_2	2	°C
6	Approaching Temperature of Condenser	ΔT_3	2	°C
7	Approaching Temperature of Generator	ΔT_4	2	°C
8	Concentration difference	ΔX	0.1	%
9	Guess Temperature (outlet of water from absorber)	T_{11}	50	°C
10	Wall superheat in evaporator	ΔT_{wse}	1	°C

Table 8
Thermodynamic properties (SI units) of state points corresponding to input data in Table 1.

State Points	Temperature (°C)	Pressure (bar)	Enthalpy (kJ/kg)	Mass flow rate (g/s)	Concentration (%)
1	52.0	0.038	109.197	1.24	50.7617
2	52.0	0.370	109.197	1.24	50.7617
3	125.5	0.370	283.133	1.04	60.7600
4	71.7	0.038	283.133	1.04	60.7600
5	88.8	0.370	2632.91	0.20	
6	74.0	0.370	117.384	0.20	
7	28.0	0.038	117.384	0.20	
8	28.0	0.038	2551.97	0.20	
9	30.0		117.384		
10	28.0		221.878	6.52	
11	51.5		215.606	6.52	
12	51.5		215.606	6.52	
13	72.0		301.398		
14	127.5				
15*	29.0				
16*	126.1				

* State point 15 and 16 corresponds to wall of evaporator and generator.

Table 9
Design specifications (SI units) corresponding to input data in Table 1.

		Evaporator	Absorber	Generator	Condenser
LMTD	(°C)	3.4761	22.2964	1.2886	8.4698
UA	(kW/°C)	0.1438	0.0311	0.5520	0.0611

Table 10
Heat pump performance (SI units) corresponding to input data in Table 1.

Qe (kW)	COP	CR	Wp (W)	T_{max} (°C)	T_{min} (°C)	P_{max} (bar)	P_{min} (bar)	X_{max} (%)	X_{min} (%)	$T_a = T_{10}$ (°C)	Σ UA (kW/°C)
0.5	0.7145	5.0762	0.156	127.54	28	0.370	0.037	60.76	50.76	28	1.0440

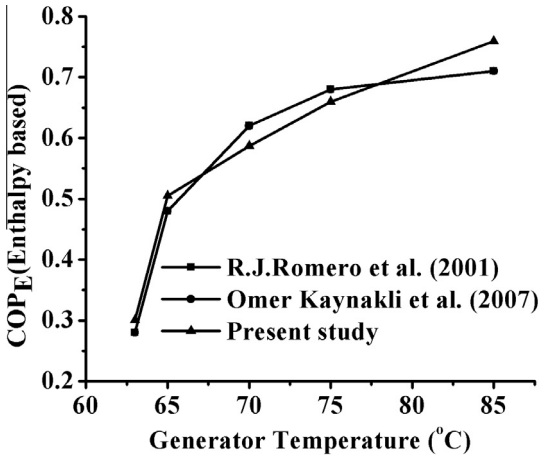

Figure 9. Comparison of COPE values.

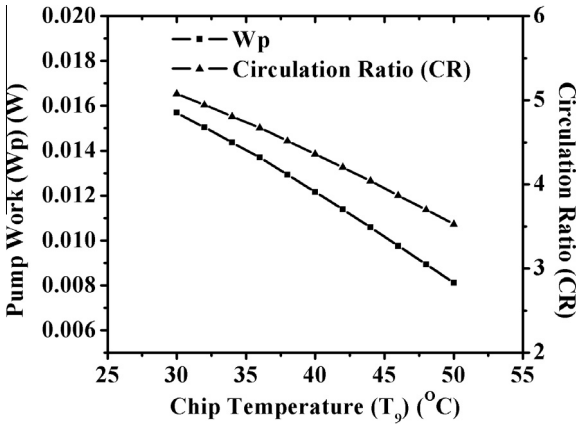

Figure 11. Comparison of Wp and CR with the Chip temperature.

pressure, but there is no effect on condenser pressure (P_3) and remains constant as 0.3700 bar due to constant condenser temperature (T_6) as 74 °C. The results of Fig. 14 are in good agreement with the reference (Joudi and Lafta, 2001). Fig. 15 demonstrates the variation of temperature as a function of T_9 at constant approaching temperatures and constant inlet cooling water temperature of 28 °C, as T_9 increases there is an decrease in heater temperature (T_{14}) from 127.541 to 95.5493 °C this is due to a decrease in concentration of the solution leaving the generator resulting in a decrease in solution temperature of the strong solution coming from the generator (generator temperature (T_3)) from 125.541 to 93.54 °C. Romera et al. (2000) showed that, generator temperature is a function of solution concentration. Similarly, there is a constant coolant outlet temperature from the absorber (T_{11}) as 51 °C, this is due to a decrease in concentration of the solution leaving the absorber at constant absorber temperature (T_1) as 52 °C and constant ΔT_2, but coolant outlet temperature from the condenser (T_{13}) remains constant as 72 °C this is due to constant condenser temperature (T_6) and ΔT_3. The results of Figs. 14 and 15 are in line with the reference (Romera et al., 2000).

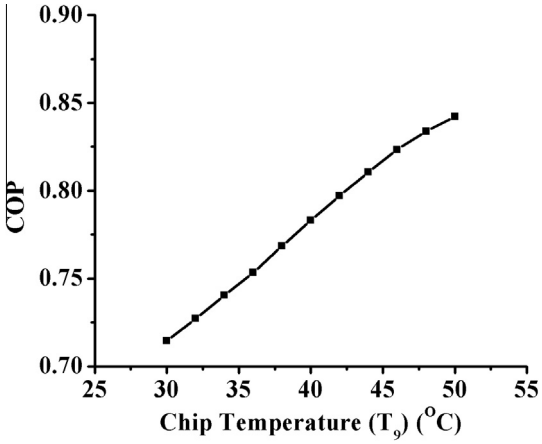

Figure 10. Variation of COP with the Chip temperature.

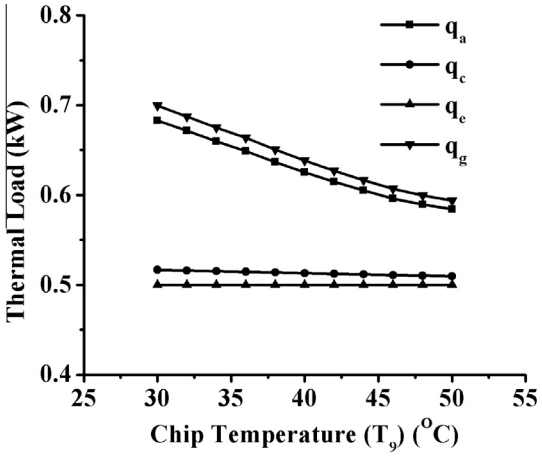

Figure 12. Variation of thermal load with the Chip temperature.

5.5. Effect of chip temperature on mass flow rate

Fig. 16 demonstrates the variation of mass flow rate as a function of T_9 at a constant approaching temperatures and constant inlet cooling water temperature of 28 °C. As T_9 increases, there is an decrease in the mass flow rates of weak solution coming from the absorber (m_1) from 1.2479 to 0.9484 g/s and a decrease in the mass flow rates of strong solution coming from the generator (m_3) from 1.0425 to 0.7389 g/s this is due to decrease in CR. Florides et al. (2003) showed a decrease in the concentration of weak solution decreases the circulation of (m_1) and this resulted in a decrease in CR but there is an increase in mass flow rate of refrigerant (m_8) from 0.2054 to 0.2095 g/s this because of an increase in the evaporator temperature and an increase in latent heat ($\Delta H = H_8 - H_7$), increase in mass flow rate of coolant (water) (m_{10}) from 6.5226 to 5.9466 g/s, this is due to a decrease in ($\dot{q}_a$) at constant ($\dot{q}_c$). The results of Fig. 16 are in good agreement with the references (Romera et al., 2000; Florides et al., 2003).

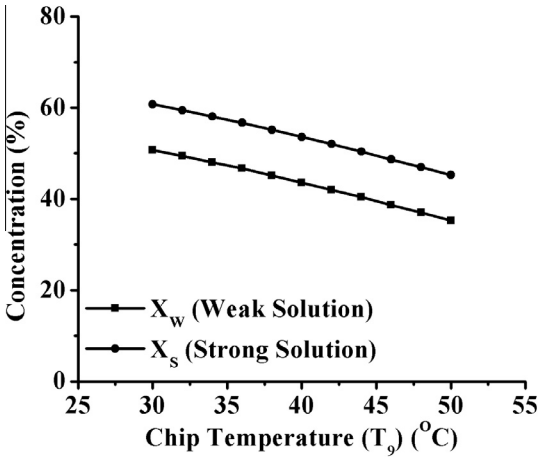

Figure 13. Variation of Concentration with the Chip temperature.

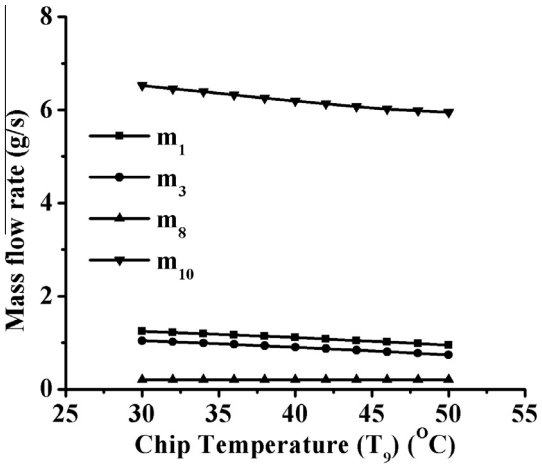

Figure 16. Variation of mass flow with the Chip temperature.

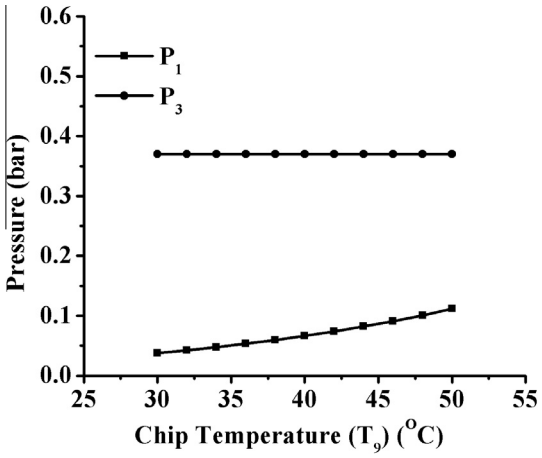

Figure 14. Variation of pressure with the Chip temperature.

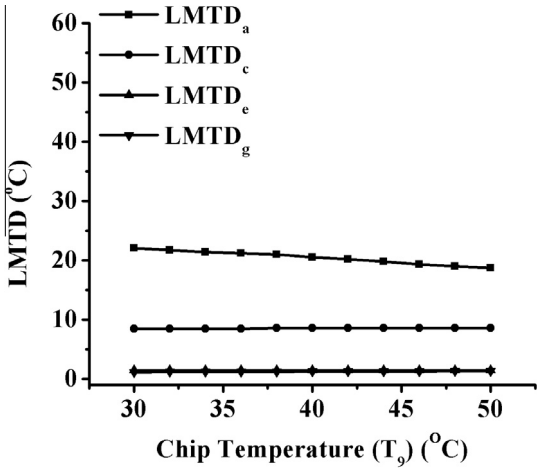

Figure 17. Variation of LMTD with the Chip temperature.

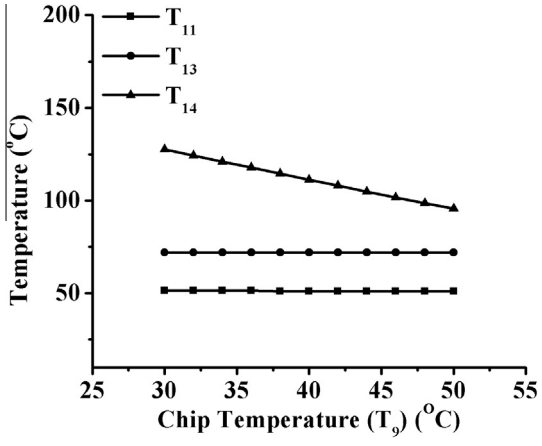

Figure 15. Variation of temperature with the Chip temperature.

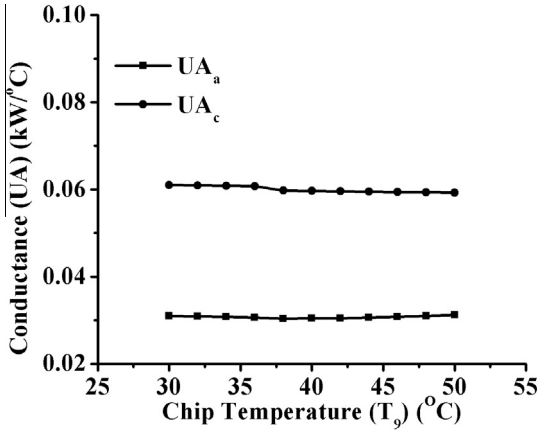

Figure 18. Variation of UA_a and UA_c with the Chip temperature.

5.6. Effect of chip temperature on LMTD and conductance

Fig. 17 demonstrates the variation of LMTD as a function of T_9 at constant approaching temperatures and constant inlet cooling water temperature of 28 °C. There is a slight decrease in trend of $LMTD_a$ from 22.0573 to 18.7260 °C because of a slight decrease in temperature of the strong solution arriving into the absorber (T_4) from

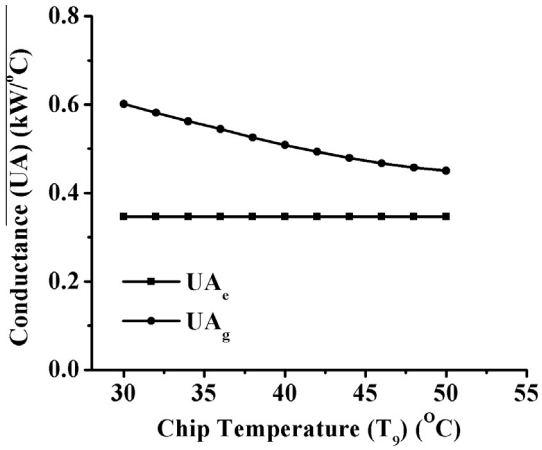

Figure 19. Variation of UA_e and UA_g with the Chip temperature.

71.7224 to 65.2877 °C due to a decrease in strong solution concentration coming from the generator but a minor increase in $LMTD_c$ from 8.469 to 8.598 °C this is due to constant coolant outlet temperature from the absorber (T_{11}) at constant T_6 and T_{13} and $LMTD_g$ varies from 1.1634 to 1.3184 °C but $LMTD_e$ remains constant as 1.4 °C. Fig. 18 shows the variation in conductance of the absorber (UA_a) and conductance of the condenser (UA_c) as a function of T_9 at constant approaching temperatures and constant inlet cooling water temperature of 28 °C. As T_9 increases, there is an increase in UA_a from 0.0310 to 0.0312 kW/°C and a decrease in UA_c from 0.0610 to 0.0593 kW/°C, this is due to a decrease in q_a and q_c, decrease in UA_g from 0.6014 to 0.4503 kW/°C which can be observed from Fig. 18, this is due to an increase in the ($\dot{q}_g$) but conductance of the evaporator (UA_e) remains unchanged as 0.3466 kW/°C which can be observed from Fig. 19 because of constant ($\dot{q}_e$).

6. Conclusions

In this study, thermodynamic analysis of the single-stage LiBr–H_2O vapor absorption heat pump for chip cooling in the non existence of solution heat exchanger was performed and additionally, a user-friendly visual software package was developed in scope of this study. The model is validated by using the values available in the literature and indicates greater reduction in the absorber load. The simulation results exhibited that the COP values rise from 0.7145 to 0.8421 with increasing chip temperature from 30 °C to 50 °C and a decrease in generator, absorber and condenser loads at constant evaporator load. Further, the CR value of the system showed its significance in deciding the performance and design of the system. It is anticipated that operations on LiBr–H_2O vapor absorption heat pump for chip cooling with respect to operating conditions, the accurate and fast computation of performance and it is possible to find suitable operating conditions and determining the effect of chip temperature on performance, loads, flow rates and conductance at fast rate with high accuracy by the developed user-friendly GUI.

References

Agrawal, Tanmay, Anoop Kumar, Varun, 2015. Solar absorption refrigeration system for air-conditioning of a classroom building in Northern India. J. Inst. Eng. (India): Series C. http://dx.doi.org/10.1007/s40032-015-0180-2.

Agyenim, F., Knight, I., Rhodes, M., 2010. Design and experimental testing of the performance of an outdoor LiBr/H_20 solar thermal absorption cooling system with a cold store. Sol. Energy 84, 735–744.

Alva, L., Gonzalez, J., 2002. Simulation of an air-cooled solar-assisted absorption air conditioning system. J. Sol. Energy Eng. 124 (3), 276–282. http://dx.doi.org/10.1115/1.1487885.

Aphornratana, S., Sriveerakul, T., 2007. Experimental studies of a single-effect absorption refrigerator using aqueous lithium-bromide: effect of operating condition to system performance. Exp. Therm. Fluid Sci. 32, 658–669. http://dx.doi.org/10.1016/j.expthermflusci.2007.08.003.

Aphornratana, S., Sriveerakul, T., 2007. Experimental studies of a single-effect absorption refrigerator using aqueous lithium–bromide: effect of operating condition to system performance. Exp. Therm. Fluid Sci. 32, 658–669. http://dx.doi.org/10.1016/j.expthermflusci.2007.08.003.

Asdrubali, F., Grignaffini, S., 2005. Experimental evaluation of the performances of a H_2O-LiBr absorption refrigerator under different service conditions. Int. J. Refrig. 28, 489–497. http://dx.doi.org/10.1016/j.ijrefrig.2004.11.006.

Atilgan, Ibrahim, Aygun, Cevdet, 2014. Simulation of double effect absorption refrigeration system. Prog. Sustainable Energy Technol. 2, 685–703. http://dx.doi.org/10.1007/978-3-319-07977-6_45.

Atmaca, A., Yigit, A., 2003. Simulation of solar-powered absorption cooling system. Renewable Energy 28, 1277–1293. http://dx.doi.org/10.1016/S0960-1481(02)00252-5.

Bin, Lu, Meng, W.J., Mei, Fanghua, 2012. Microelectronic chip cooling: an experimental assessment of a liquid-passing heat sink, a microchannel heat rejection module, and a microchannel-based recirculating-liquid cooling system. Microsyst. Technol. 18 (2), 341–352. http://dx.doi.org/10.1007/s00542-011-1397-5.

Bintoro, J.S., Akbarzadeh, A., Mochizuki, M., 2005. A closed-loop electronics cooling by implementing single phase impinging jet and mini channels heat exchanger. Appl. Therm. Eng. 25, 2740–2753. http://dx.doi.org/10.1016/j.applthermaleng.2005.01.018.

Cantarutti, Bruno Ribeiro, 2011. Theoretical-experimental analysis of a cooling system for absorption effect using simple Libr–H_2O (Master Thesis). Federal university of Itajuba Institute of Mechanical Engineering Graduate program in Mechanical Engineering, http://saturno.unifei.edu.br/bim/0038210.pdf.

Chaudhari, S.K., Paranjape, D.V., Eisa, M.A.R., Holland, F.A., 1985. A study of the operating characteristics of a Water–Lithium Bromide absorption heat pump. Heat Recovery Syst. 5 (4), 285–297. http://dx.doi.org/10.1016/0198-7593(85)90003-7.

Chiriac, Victor, Chiriac, Florea, 2010. Absorption refrigeration method with alternative water-ammonia solution circulation system for microelectronics cooling. Proceedings of ITHERM 2010, 2nd–5th June 2010, Las Vegas, NY. http://dx.doi.org/10.1109/ITHERM.2010.5501391.

Coggins, C., Gerlach, D., Joshi, Y., Fedorov, A., 2006 Compact, low temperature refrigeration of microprocessors. In: International Refrigeration and Air Conditioning Conference at Purdue, Paper No. R064, West Lafayette, IN, July 15-20. http://docs.lib.purdue.edu/iracc/814/.

Cunha, Francisco Ricardo, Couto, H.L.G., Marcelino, N.B., 2007. A study on magnetic convection in a narrow rectangular cavity. Magnetohydrodynamics 43 (8), 421–428, http://adsabs.harvard.edu/abs/2007MHD....43..421C.

Ebrahimi, Khosrow, Jones, Gerard F., Fleischer, Amy S., 2015. Thermo-economic analysis of steady state waste heat recovery in data centers

using absorption refrigeration. Appl. Energy 139 (1), 384–397. http://dx.doi.org/10.1016/j.apenergy.2014.10.067.

Eisa, M.A.R., Holland, F.A., 1986. A study of the operating parameters in a water-lithium bromide absorption cooler. Int. J. Energy Res. 10 (2), 137–144. http://dx.doi.org/10.1002/er.4440100204.

Eisa, M.A.R., Devotta, S., Holland, F.A., 1986. Thermodynamic design data for absorption heat pump systems operating on water-Lithium bromide: Part I-cooling. Appl. Energy 24, 287–301. http://dx.doi.org/10.1016/0306-2619(86)90068-1.

Fan, X., Zeng, G., LaBounty, C., Bowers, J.E., Croke, E., Ahn, C.C., Huxtable, S., Majumdar, A., Shakouri, A., 2001. SiGeC/Si superlattice microcoolers. Appl. Phys. Lett. 78 (11), 1580–1582. http://dx.doi.org/10.1063/1.1356455.

Florides, G.A., Kalogirou, S.A., Tassou, S.A., Wrobel, L.C., 2003. Design and construction of a LiBr–water absorption machine. Energy Convers. Manage. 44, 2483–2508. http://dx.doi.org/10.1016/S0196-8904(03)00006-2.

França, Francis Henrique Ramos, dos Santos, Elizaldo D., Isoldi, Liércio A., Petry, Adriane P., 2014. A numerical study of combined convective and radiative heat transfer in non-reactive turbulent channel flows with several optical thicknesses: a comparison between LES and RANS. J. Braz. Soc. Mech. Sci. Eng. 36 (1), 207–219. http://dx.doi.org/10.1007/s40430-013-0075-1.

França, Francis Henrique Ramos, Zhao, Y., Molki, M., Ohadi, M.M., Radermacher, R., 2002. Flow Boiling of CO_2 with Miscible Oil in Microchannels. ASHRAE Trans. 108 (1), 135–144, http://www.techstreet.com/products/1719532.

García Cascales, J.R., Vera García, F., Cano Izquierdo, J.M., Delgado Marín, J.P., Martínez Sánchez, R., 2011. Modelling an absorption system assisted by solar energy. Appl. Therm. Eng. 31, 112–118. http://dx.doi.org/10.1002/er.4440100204.

Grossman, Gershon, Zaltash, Abdi, 2001. ABSIM-modular simulation of advanced absorption systems. Int. J. Refrig. 24 (6), 531–543. http://dx.doi.org/10.1016/S0140-7007(00)00051-7.

Hewitt, Neil, Agyenim, Francis, Eames, Philip, Smyth, Mervyn, 2010. A review of materials, heat transfer and phase change problem formulation for latent heat thermal energy storage systems (LHTESS). Renew. Sustain. Energy Rev. 14 (2), 615–628. http://dx.doi.org/10.1016/j.rser.2009.10.015.

Magnus Holmgren, 2006. http://in.mathworks.com/matlabcentral/fileexchange/9817-x-steam–thermodynamic-properties-of-water-and-steam.

Incopera, Dewitt, Bergman, Lavine, 2007. Fundamental of Heat and Mass Transfer, 6th ed. John Wiley and Sons.

Iranmanesh, A., Mehrabian, M.A., 2012. Thermodynamic modelling of a double-effect LiBr–H_2O absorption refrigeration cycle. Heat Mass Transfer 48 (12), 2113–2123. http://dx.doi.org/10.1007/s00231-012-1045-3.

Jiang, L., Mikkelsen, J., Koo, J.M., Huber, D., Yao, S., Zhang, L., Zhou, P., Maveety, J.G., Prasher, R., Santiago, J.G., Kenny, T.W., Goodson, K.E., 2002. Closed-loop electroosmotic microchannel cooling system for VLSI circuits. IEEE Trans. Comp. Packag. Technol. 25 (3), 347–355. http://dx.doi.org/10.1109/TCAPT.2002.800599.

Joudi, Khalid A., Lafta, Ali H., 2001. Simulation of a simple absorption refrigeration system. Energy Convers. Manage. 42, 1575–1605. http://dx.doi.org/10.1016/j.solener.2010.01.013.

Karno, Ali, Ajib, Salman, 2008. Thermodynamic analysis of an absorption refrigeration machine with new working fluid for solar applications. Heat Mass Transfer 45 (1), 71–78. http://dx.doi.org/10.1007/s00231-008-0408-2.

Kaynakli, Omer, Kilic, Muhsin, 2007. Theoretical study on the effect of operating conditions on performance of absorption refrigeration system. Energy Convers. Manage. 48, 599–607. http://dx.doi.org/10.1016/j.enconman.2006.06.005.

Kim, Yoon Jo, Joshi, Yogendra K., Fedrov, Andrei G., 2008. An absorption based miniature heat pump system for electronics cooling. Int. J. Refrig. 31, 23–33. http://dx.doi.org/10.1016/j.ijrefrig.2007.07.003.

Lee, S.F., Sherif, S.A., 2000. Thermodynamic analysis of a lithium bromide/water absorption system for cooling and heating applications. Int. J. Energy Res. 25, 1019–1031. http://dx.doi.org/10.1002/er.738.

Marc, O., Lucas, F., Sinama, F., Monceyron, E., 2010. Experimental investigation of a solar cooling absorption system operating without any backup system under tropical climate. Energy Build. 2, 774–782. http://dx.doi.org/10.1016/j.expthermflusci.2007.08.003.

Martinez, P., Pinazo, J., 2002. A method for design analysis of absorption machines. Int. J. Refrig. 25 (5), 634–639. http://dx.doi.org/10.1016/S0140-7007(01)00052-4.

Maydanik, Y.F., Vershinin, S.V., Korukov, M.A., Ochterbeck, J.M., 2005. Miniature loop heat pipes – a promising means for electronics cooling. IEEE Trans. Comp. Packag. Technol. 28 (2), 290–296. http://dx.doi.org/10.1109/TCAPT.2005.848487.

Mehrabian, M.A., Shahbeik, A.E., 2005. Thermodynamic modelling of a single-effect LiBr–H_2O absorption refrigeration cycle. Proc. Inst. Mech. Eng., Part E: J. Process Mech. Eng. 219 (3), 261–273. http://dx.doi.org/10.1243/095440805X8656.

Melograno, P., Santiago, J., Franchini, G., Sparber, W., 2009. Experimental analysis of a discontinuous sorption chiller operated in steady conditions. 3rd International Conference Solar Air Conditioning Proceedings, Palermo, Italy, http://www.researchgate.net/publication/228607232_Experimental_Analysis_of_a_Discontinuous_Sorption_Chiller_Operated_in_Steady_Conditions.

Mongia, R., Masahiro, K., DiStefano, E., Barry, J., Chen, W., Izenson, M., Possamai, F., Zimmermann, A., Mochizuki, M., 2006. Small scale refrigeration system for electronics cooling within a notebook computer. ITHERM'06, Proceedings of the Tenth Intersociety Conference on Thermal and Thermo mechanical Phenomena in Electronics Systems, San Diego, USA, pp. 751–758. http://dx.doi.org/10.1109/ITHERM.2006.1645421.

Mostafavi, M., Agnew, B., 1996. The impact of ambient temperature on lithiumbromide/water absorption machine performance. Appl. Therm. Eng. 16 (6), 515–522. http://dx.doi.org/10.1016/1359-4311(95)00004-6.

Mudawar, Issam, 2011. Two-phase microchannel heat sinks: theory, applications, and limitations. J. Electron. Packag. 133, 1–31. http://dx.doi.org/10.1115/1.4005300.

Mudawar, Issam, Weilin, Qu, 2005. A systematic methodology for optimal design of two-phase micro-channel heat sinks. J. Electron. Packag. 127, 381–390. http://dx.doi.org/10.1115/1.2056571.

Pal, A., Joshi, Y.K., Beitelmal, M.H., Patel, C.D., Wenger, T.M., 2002. Design and performance evaluation of a compact thermosyphon. IEEE Trans. Comp. Packag. Technol. 25 (4), 601–607. http://dx.doi.org/10.1109/TCAPT.2002.807997.

Pongtornkulpanich, A., Thepa, S., Amornkitbamrun, M., Butcher, C., 2008. Experience with fully operational solar-driven 10-ton LiBr/H_2O single-effect absorption cooling system in Thailand. Renewable Energy 33, 943–949. http://dx.doi.org/10.1016/j.renene.2007.09.022.

Qi, Zhaogang, Chen, Jiangping, Radermacher, Reinhard, 2009. Investigating performance of new mini-channel evaporators. Appl. Therm. Eng. 29 (17–18), 3561–3567. http://dx.doi.org/10.1016/j.applthermaleng.2009.06.011.

Ribeiro, Guilherme B., Barbosa Jr., Jader R., Prata, Alvaro T., 2010. Mini-channel evaporator/heat pipe assembly for a chip cooling vapor compression refrigeration system. Int. J. Refrig. 33 (7), 1402–1412. http://dx.doi.org/10.1016/j.ijrefrig.2010.05.010.

Romera, R.J., Rivera, W., Best, R., 2000. Comparison of the theoretical performance of a solar air conditioning system operating with water/lithium bromide and an aqueous ternary hydroxide. Solar Energy Mater. Solar Cells 63 (3), 87–99. http://dx.doi.org/10.1016/S0927-0248(00)00058-1.

Rubio-Maya, Carlos, Pacheco-Ibarra, J.Jesús., Belman-Flores, Juan M., Galván-González, Sergio R., Mendoza-Covarrubias, Crisanto., 2012. NLP model of a LiBreH2O absorption refrigeration system for the minimization of the annual operating cost. Appl. Therm. Eng. 37, 10–18.

Sedighi, K., Farhadi, M., Liaghi, M., 2007. Exergy analysis: parametric study on lithium bromide—water absorption refrigeration systems.

Proc. Inst. Mech. Eng., Part C: J. Mech. Eng. Sci. 221 (11), 1345–1351. http://dx.doi.org/10.1243/09544062JMES604.

Sencana, Arzu, Yakut, Kemal A., Kalogirou, Soteris A., 2005. Exergy analysis of lithium bromide/water absorption systems. Renewable Energy 30, 645–657. http://dx.doi.org/10.1016/j.renene.2004.07.006.

Talbi, M.M., Agnew, B., 2000. Exergy analysis: an absorption refrigerator using lithium bromide and water as the working fluids. Appl. Therm. Eng. 20, 619–630. http://dx.doi.org/10.1016/S1359-4311(99)00052-6.

Tan, F.L., Tso, C.P., 2004. Cooling of mobile electronic devices using phase change materials. Appl. Therm. Eng. 24, 159–169. http://dx.doi.org/10.1016/j.applthermaleng.2003.09.005.

Trutassanawin, Suwat, Groll, Eckhard A., Garimella, Suresh V., Cremaschi, Lorenzo, 2006. Experimental investigation of a miniature-scale refrigeration system for electronics cooling. IEEE Trans. Compon. Packag. Technol. 29, 678–687. http://dx.doi.org/10.1109/TCAPT.2006.881762.

Tuckerman, D.B., Pease, R.F.W., 1981. High-performance heat sinking for VLSI. IEEE Electron Devices Lett. 5, 126–129. http://dx.doi.org/10.1109/EDL.1981.25367.

Vargas, J.V.C., Horuz, I., Callander, T.M.S., Fleming, J.S., Parise, J.A.R., 1988. Simulation of the transient response of heat driven refrigerators with continuous temperature control: simulation de la réponse transitoire des réfrigérateurs utilisant une source de chaleur avec maîtrise de la température en continu. Int. J. Refrig. 21 (8), 648–660. http://dx.doi.org/10.1016/S0140-7007(98)00009-7.

Yang, W.-J., Guo, K.H., 1987. Solar-assisted lithium-bromide absorption cooling systems. Solar Energy Utilization NATO ASI Series 129, 409–423. http://dx.doi.org/10.1007/978-94-009-3631-7_19.

Yoon, Jung-In, Choi, Kwang-Hwan, Moon, Choon-Geun, Kim, Young Jin, Kwon, Oh-Kyung, 2003. A study on the advanced performance of an absorption heater/chiller with a solution preheater using waste gas. Appl. Therm. Eng. 23, 757–767. http://dx.doi.org/10.1016/S1359-4311(03)00003-6.

Yoon Jo Kim, Yogendra K. Joshi, Andrei G. Fedorov, 2007. Design of an Absorption Based Miniature Heat Pump System for Cooling of High Power Microprocessors, IPACK2007-33245:69–77. DOI:10.1115/IPACK2007-3324.